JOURNAL OF MATERIALS SCIENCE 29 (1994) 929–933

Comparison of structure and properties of alloys in amorphous, nanocrystalline and coarse-grained polycrystalline states

X. D. LIU, J. T. WANG, J. ZHU*
*State Key Laboratory of RSA, Institute of Metal Research, and *International Centre for Materials Physics, Academia Sinica, Shenyang 110015, People's Republic of China*

Some properties, including the microhardness, H_v, and electrical resistivity of a nanocrystalline, two coarse-grained polycrystalline and one amorphous alloys of Fe–Mo–Si–B of the same composition, were measured experimentally and compared. The structures of amorphous, nanocrystalline and coarse-grained Fe–Mo–Si–B alloys are also compared and discussed.

1. Introduction

Since the first report by Birringer *et al.* [1, 2], a new catalogue of materials, called nanocrystalline materials with ultrafine particles sized from 1–100 nm, has been successfully synthesized by means of the inert-gas condensation [3], ball-milling [4], or severe torsional plastic deformation [5], etc. It is of interest to compare the structure and properties of amorphous, nanocrystalline as well as coarse-grained polycrystalline materials with the same chemical composition. A new method for preparing bulk nanocrystalline alloys from metallic glasses which was developed by our laboratory [6], makes it possible to generate directly bulk materials with various grain sizes. It involves the formation of amorphous ribbons, wires or powders as raw material, then by appropriate heat treatments, nanocrystallites will nucleate and grow from the amorphous matrix. To obtain nanocrystalline materials, knowledge about the crystallization behaviour of an amorphous alloy is required.

A remarkable characteristic, different from normal coarse-grained crystals or traditional glasses, is the existence of a large number of interfaces and a substantial number of atoms situated in grain boundaries. The atomic arrangements in grain boundaries directly affect the structure and properties of interfaces and then correspondingly exert considerable influence on the properties of materials. It was proved that the thermal expansion coefficient of grain boundaries is about two to five times larger than that of crystals [1, 2] and an inverse Hall–Petch relation was found by Lu *et al.* [7] and Schaefer and Wurschum [8]. Therefore, the investigation of interfaces in nanocrystalline materials has always been a great challenge. The structures of nanocrystalline materials have been studied using positron annihilation (PA) [9], Mössbauer spectroscopy (MES) [10], and high-resolution electronic microscopy (HREM) [11], etc.

A direct comparison of structure and properties of materials in three states: amorphous, nanocrystalline and coarse-grained, with the same composition of $(Fe_{0.99}Mo_{0.01})_{78}Si_9B_{13}$ (at %), was made in this work.

2. Experimental procedure

2.1. Sample preparation

Amorphous $(Fe_{0.99}Mo_{0.01})_{78}Si_9B_{13}$ (at %) ribbons of 3–5 mm width and about 27 μm thickness, were prepared by the melt-spinning technique. Two crystallization steps were observed on DSC curve (Perkin–Elmer, DSC-2) during heating the as-quenched sample at a rate of 20 K min^{-1}. The peak temperatures of crystallization are 841.0 (T_{p_1}) and 858.0 K (T_{p_2}), respectively

The annealing treatments for producing nanocrystallites were as follows. A tubular furnace was preheated to the required temperature under an argon stream before placing the as-quenched ribbons in it. After annealing had finished, the as-annealed samples were immediately removed from the furnace and quenched into water.

2.2 Structure and properties

The as-annealed samples were studied by X-ray diffraction (XRD) on a Rigaku X-ray diffractometer, using CuK_α radiation, and TEM on a Philips EM 420 microscope, to identify the crystalline phases as well as to observe the morphologies and grain sizes.

The structures of the materials in the three states were investigated using positron annihilation (PA), on a fast–fast coincidence ORTEC system, and Mössbauer spectroscopy (MES) on a computer-controlled Mössbauer spectrometer.

The microhardness, H_v, measurements were done on a microhardness tester with a load of 50 g and a test time of 10 s. The samples were polished to remove the flaws in the surface before the test. The electrical resistivity was measured at room temperature using the four-probe method.

0022–2461

3. Results and discussion

3.1. XRD and TEM

Table I lists the tested samples and the average grain sizes determined from TEM observations. For comparison, the results for the as-cast sample are also presented (the as-cast specimen was annealed at 913 K for 2 h).

Fe–Mo–Si–B alloys in the three states were characterized by XRD as shown in Fig. 1. The as-quenched sample was confirmed to be in the amorphous state (Fig. 1a). On heating the as-quenched sample at 833 K for 1 h, fully crystallized state was observed with precipitation of α-Fe(Si,Mo) (b c c) solution as well as $(Fe,Mo)_{23}B_6$ (f c c), $(Fe,Mo)_3B$ (b c t) and Fe_2B (b c t) borides (Fig. 1b). However, when the annealing temperature reaches 1023 K, no trace of $(Fe,Mo)_{23}B_6$ and $(Fe,Mo)_3B$ can be detected (Fig. 1c), indicating that, at higher temperatures, transformation from metastable $(Fe,Mo)_{23}B_6$ and $(Fe,Mo)_3B$ to α-Fe and Fe_2B phases occurs. Only two crystalline phases were found in the as-cast sample (Fig. 1d), so we infer that at least three metastable phases appear during the crystallization and grain growth of FeMoSiB alloy; they are $(Fe,Mo)_3B$, $(Fe,Mo)_{23}B_6$ and $(Fe,Mo)_3Si$.

Fig. 2 shows transmission electron micrographs for the samples annealed at 833 K (Fig. 2a) and 1023 K (Fig. 2b) for 1 h. It is interesting that ultrafine grains of about 15 nm were observed in the sample annealed at 833 K for 1 h; no dendrites appear. However, with increasing annealing temperature, the grains become coarse and polygonal grains are developed (Fig. 2b). The average grain size is about 200 nm. At that time, the grains are much more heterogeneous than that in Fig. 2a.

TABLE I The average grain sizes for the tested samples

	A	B	C	D
Sample	Amorphous	Nanocryst. (833 K, 1 h)	Coarse-grained (1023 K, 1 h)	As-cast (913 K, 2 h)
Grain size(nm)		15	200	$> 10^3$

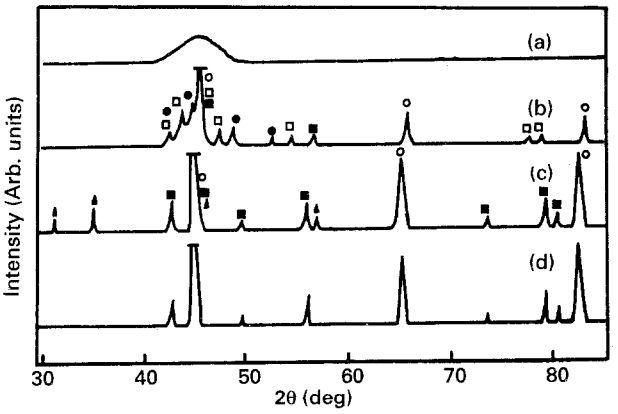

Figure 1 XRD patterns of (a) amorphous, (b) nano crystalline, (c) coarse-grained, and (d) as-cast samples. (○) α-Fe(Si, Mo), (●) (Fe, Mo)$_{23}$B$_6$, (□) (Fe, Mo)$_3$B, (▲) (Fe, Mo)$_3$Si, (■) Fe_2B.

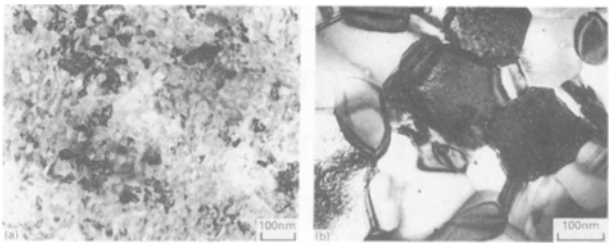

Figure 2 Bright-field transmission electron micrographs of (a) nanocrystalline and (b) coarse-grained samples

It is worth mentioning that the crystallization of amorphous Fe–Mo–Si–B alloy and the growth of nanocrystallites are quite different. As discussed by Liu and Wang [12], almost simultaneous precipitation of four crystalline phases, as shown in Fig. 1b, takes place when heating the as-quenched sample at a constant rate. Crystallization proceeds within a very narrow temperature interval. However, the growth of nanocrystallites is more complicated in that complex phases co-exist over a long-temperature range 813–913 K [12] and phase transformations are accompanied by grain growth.

3.2. Properties

Table II lists microhardness and electrical resistivity of the tested samples. Obviously, both H_v and ρ_{RT} of the nanocrystalline sample are larger than those of amorphous, coarse-grained crystal and as-cast samples, which might be attributed to the complicated structures of grain and/or phase boundaries. It is of great interest that microhardness, H_v, does not vary monotonically with the average grain size. It shows an obvious critical phenomenon [13]. The variation of H_v with respect to $\bar{D}$ can be written as

$$H_v(\text{GPa}) = 4.28\ \text{GPa} + 36.2(\text{GPa nm}^{1/2})\ \bar{D}^{-1/2}(\text{nm}^{-1/2}) \quad \bar{D} > 45\ \text{nm} \quad (1)$$

$$= 13.75\ \text{GPa} - 23.77(\text{GPa nm}^{1/2})\ \bar{D}^{-1/2}(\text{nm}^{-1/2}) \quad \bar{D} < 45\ \text{nm} \quad (2)$$

The volume percentage of atoms in the interfaces is

$$C_i = 3\delta/(d + \delta)$$

where δ is the average width of grain boundaries and d the average diameter of crystallites. With grain growth, the grain and phase boundaries shrink, which is suggested to be detrimental to H_v and ρ_{RT}. However, when D is less than 45 nm, the deformation mechanism is unclear, requiring further investigation in that an inverse Hall–Petch effect exists instead of the normal one, as shown in Equation 2.

3.3. Positron annihilation results

Positron lifetime spectroscopy has proved to be a powerful tool to investigate the defective structure of a material. Table III lists the PA results for the samples in three states. The spectra for the crystallized samples

TABLE II Properties of the tested samples

Samples	H_v (GPa)	ρ_{RT}(μΩm)
A	6.4 ± 0.3	1.96 ± 0.1
B	8.4 ± 0.3	2.00 ± 0.1
C	6.3 ± 0.3	0.63 ± 0.1
D	5.6 ± 0.2	0.40 ± 0.1

were fitted by using three exponents, while for the as-quenched sample, two lifetimes are obtained after source and background corrections.

The shorter lifetime, τ_1, of the amorphous sample is much larger than the lifetime of positrons annihilated in the delocalized free state, τ_f, in the corresponding bulk sample, and shorter than that at monovacancy, τ_{1v}. For bulk iron, $\tau_f = 106$ ps, $\tau_{1v} = 170$ ps. For the as-quenched sample, τ_1 is due to the thermolization positrons being completely trapped by quenched-in free volumes in the amorphous sample and is annihilated in these defects. This kind of defect can also be termed a Bernal hole, of which the size is smaller than a monovacancy. So it is a shallow trapping potential compared with a monovacancy. In comparison with a molybdenum free sample, which shows $\tau_1 = 150.0$ ps and $I_1 = 98.6\%$, the addition of elemental molybdenum almost makes no difference to the amorphous structure of FeSiB glass.

From Table III, one can see that the long lifetime, τ_3, is larger than 1500 ps, and its intensity is less than 2.0%. This results from positron annihilation in very large voids (1 μm diameter). TEM results demonstrate that no such large voids exist in the amorphous and crystallized samples. Typical examples are shown in Fig. 2a and b. Therefore, it may be caused by positrons annihilated in the surfaces of the samples and source. Thus τ_3 is related to surface factors, providing no information on the internal structure of both amorphous and crystalline samples.

In the interfaces of nanocrystalline alloys, two kinds of defect exist [14, 15], free volume-sized and microvoid-sized defects; the latter are formed by the aggregation of free volumes and are usually situated at the intersections of two or three boundaries. In the case of sample B, the intermediate lifetime, τ_2, is caused by positron annihilation in clusters of free volumes, of which the size is several diameters of a monovacancy. When the grain size increases to 200 nm, the volume percentage of grain and phase boundaries decreases rapidly. At that time, τ_1 reflects the annihilation in grains because the average grain size is larger than the mean diffusion length of positrons in perfect crystals ($L^+ = 100$ nm). In the case of sample C, τ_2 is close to that of sample B, indicating that the clusters of free volumes do not disappear even after sufficient annealing. Therefore, this kind of defect can be regarded as an intrinsic characteristic, which cannot be annealed out. However, compared with sample B, the intensity of τ_2 is increased by 5.3%, so the technical procedure of amorphous crystallization exert great influence on the structure and the state of defects.

For sample D, the shorter lifetime, τ_1, reflects positron annihilation in grains, and the intermediate lifetime, τ_2, is attributed to positron annihilation in defects such as vacancies, dislocations and grain boundaries, etc. Furthermore, a great difference in τ_1 and τ_2 and the corresponding intensities of samples B, and C, prepared by amorphous crystallization, as well as the as-cast sample, are observed. Because the values of τ_1 and τ_2 are much lower than that of sample C, and the intensity of τ_2 increases remarkably, we can see that the defective structure of the amorphous sample cannot recover to that in the casting state through crystallization.

On the other hand, microhardness and electrical resistivity of the tested samples are closely related to the defective structure. From Tables II and III, one can see that the variations of H_v and ρ_{RT} with respect to the average grain size are compatible with that of I_1/I_2, i.e. the lower the density of microvoid-sized defects, the greater is the microhardness and electrical resistivity of a material.

3.4. Mössbauer spectroscopy

Fig. 3 shows Mössbauer spectra for samples A, B, and C. It is very clear that the spectrum for the as-quenched sample consists of six well-defined but broadened peaks (Fig. 3a). The spectrum for the nanocrystalline sample is somewhat similar to that for glass (Fig. 3b). However, the spectrum for the coarse-grained sample is quite different from Fig. 3a and b, showing complicated peaks (Fig. 3c).

Fig. 4 illustrates three $P(H)$–H curves corresponding to the three spectra in Fig. 3. The curve for the as-quenched sample shows a continuous distribution feature, the mean hyperfine magnetic field $\bar{H}_{hf}$, is calculated to be about 231.1 kOe from $\bar{H}_{hf} = \int P(H)\, dH$. It is interesting that the $P(H)$–H curve for the nanocrystalline sample exhibits a quasi-continuous distribution feature, similar to that for the amorphous sample, which can be ascribed to the existence of a larger number of interfaces, on which the atoms are

TABLE III PA characteristic parameters for the tested samples

	τ_1, (ps)	τ_2, (ps)	τ_3, (ps)	I_1	I_2	I_1/I_2	I_3
A	151.0 ± 0.4		1517 ± 276	98.7 ± 1.2			1.33 ± 0.10
B	142.0 ± 1.5	240 ± 12	1582 ± 200	91.3 ± 1.0	7.4 ± 1.5	12.3	1.30 ± 0.10
C	126.3 ± 1.5	250 ± 10	1685 ± 220	85.7 ± 1.1	12.7 ± 1.4	6.75	1.60 ± 0.10
D	119.0 ± 1.2	185 ± 11	1667 ± 238	83.3 ± 1.0	15.4 ± 1.3	5.41	1.32 ± 0.12

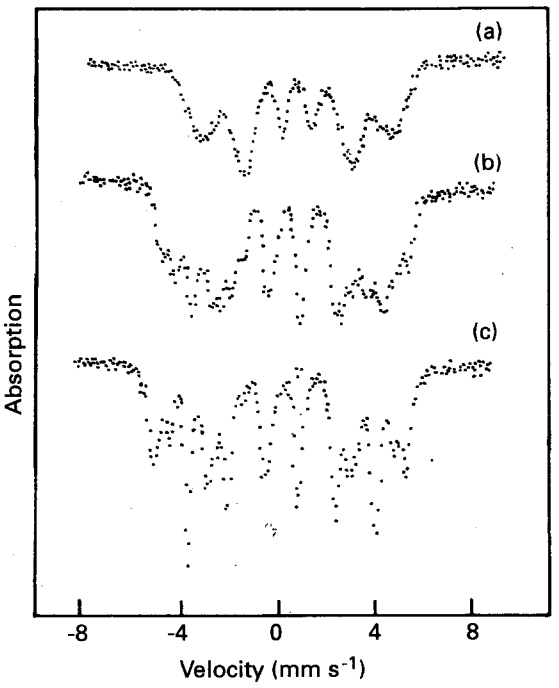

Figure 3 Mössbauer spectra of samples (a) A, (b) B and (c) C.

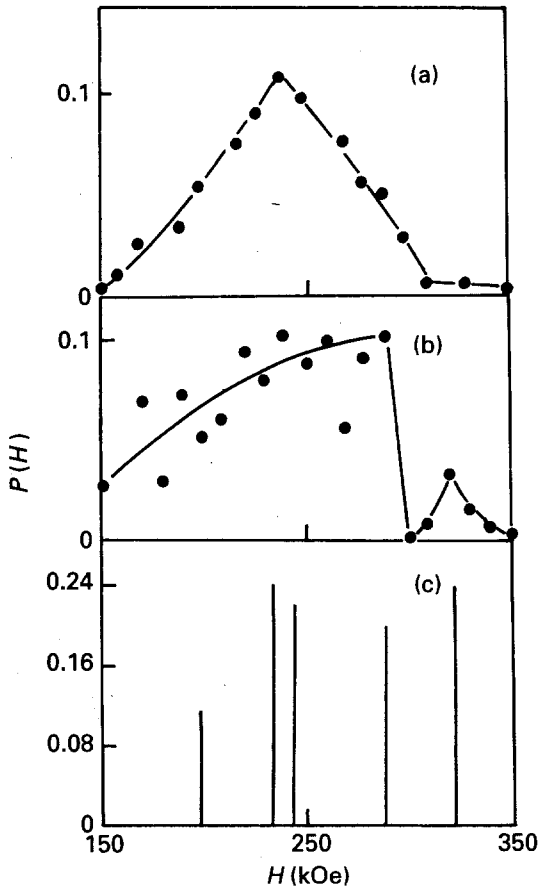

Figure 4 $P(H)$–H curves corresponding to the Mössbauer spectra in Fig. 3: (a) sample A, (b) sample B, and (c) sample C.

claimed to lack both long-range and short-range ordering [1].

The hyperfine magnetic field is thought to be sensitive to different interatomic displacements and coordinations. Therefore the quasi-continuous distribution of the hyperfine magnetic field may result from ^{57}Fe atoms at grain boundaries, which are claimed to lack ordering. Because of this special interface structure, the nanocrystalline sample shows larger H_v and ρ_{RT} than the glass and coarse-grained samples with the same composition. The peak in Fig. 4b at about 320 kOe corresponds to Fe8NN + Fe7NN.

TABLE IV MES parameters for three types of alloys

Phase	H_{hf}(kOe)	IS(mm s^{-1})	SQ(mm s^{-1})	Area(%)
Fe8NN + Fe7NN	321.4	− 0.1178	0.0423	23.5
Fe6NN	288.4	− 0.08	0.04	19.6
Fe5NN	243.0	− 0.0084	0.0521	21.6
$(Fe,Mo)_3Si$	196.0	0.0861	0.0384	11.5
Fe_2B	233.5	− 0.0688	0.068	23.8

Notes: IS is relative to the ^{57}Co source. For α-Fe(Si) phase, the Fe8NN line was not separated from Fe7NN.

The $P(H)$–H curve for the coarse-grained sample becomes discrete, composed of five separate lines corresponding to different iron configurations. The fitted results with reference to Sterns [16] are summarized in Table IV.

Owing to the solubility of silicon and molybdenum atoms in the bcc iron lattice, the surrounding environments of iron atoms change significantly, leading to four iron sites, as denoted by Fe8NN + Fe7NN, 6NN and Fe5NN. The isomer shift increases with decrease of coordination numbers, implying the reduction in density of s electrons of iron nuclei [17].

From the above discussion we can conclude that the structure and properties of a nanocrystalline Fe–Mo–Si–B sample prepared by the crystallization method, are quite different from those of amorphous and coarse-grained polycrystalline samples although their compositions are the same. The defective structure cannot recover to that in the cast state through crystallization, because the clusters of free volumes cannot be eliminated by annealing. It should be mentioned that the technical procedure of crystallization exerts a great influence on the structure and properties of the crystallized sample, especially when the grain size is quite small.

References

1. R. BIRRINGER, U. HERR and H. GLEITER, *Trans. Jpn Inst. Metals Suppl.* **27** (1986) 43.
2. R. BIRRINGER, *Mater. Sci. Engg.* **A117** (1989) 33.
3. C. G. GRANQUIST, and R. A. BUHRMAN, *J. Appl. Phys.* **47** (1976) 2200.
4. H. J. FECHT, E. HELLSTERN, Z. FU and W. L. JOHNSON, *Metall. Trans.* **A21** (1990) 2333.
5. N. A. SMIRNOVA, V. I. LEVIT, V. I. PILYGIN, R. I. KUSNETSOV, L. S. DAVIDOVA and V. A. SAZNOVA, *Phys. Met. Metall.* **61** (1990) 522
6. K. LU, J. T. WANG and W. D. WEI, *J. Appl. Phys.* **69** (1991) 522
7. A. H. CHOKSHI, A. ROSEN, J. KARCH and H. GLEITER, *Scripta Metall.* **23** (1989) 1679.
8. K. LU, W. D. WEJ and J. T. WANG, *Scripta. Metall. Mater.* **24** (1990) 2319.

9. H. E. SCHAEFER and R. WURSCHUM, *Phys. Lett.* **A119** (1987) 370.
10. R. BIRRINGER, H. GLEITER, H. P. KLEIN and P. MARQUARDT, *Ibid.* **102A** (1984) 365.
11. M. L. SUI, K. LU and Y. Z. HE, *Philos. Mag.* **B63** (1991) 993.
12. X. D. LIU and J. T. WANG, *J. Nanostructured Mater.***2** (1993) 63.
13. X. D. LIU, J. T. WANG and B. Z. DING, *Scripta Metall. Mater.* **28** (1993) 59.
14. H. E. SCHAEFER and R. WURSCHUM, *Phys. Lett.* **A119** (1987) 370.
15. R. MURCHUM, M. SCHEYTT and H. E. SCHAEFER, *Phys. Status Solidi* **102** (1987) 119.
16. M. B. STERNS, *Phys. Rev.* **129** (1963) 1136.
17. U. GONSER, "Mossbauer Spectroscopy" (Springer, Heidelberg New York, 1975).

Received 28 October 1992
and accepted 8 June 1993